

Original paper

Ti⁴⁺ and Sn⁴⁺-bearing tourmalines – pressure control and comparison of synthetic and natural counterparts

Oleg S. VERESHCHAGIN^{1,*}, Bernd WUNDER², Ivan A. BAKSHEEV³, Franziska D.H. WILKE², Natalia S. VLASENKO⁴, Olga V. FRANK-KAMENETSKAYA¹

¹ Institute of Earth Sciences, Saint Petersburg State University, Universitetskaya Emb. 7/9, 199034 St. Petersburg, Russia; o.vereshchagin@spbu.ru

² GFZ German Research Centre for Geosciences, 14473 Potsdam, Germany

³ Geological Faculty, Lomonosov Moscow State University, Leninskie Gory, 119991 Moscow, Russia

⁴ Centre for Geo-Environmental Research and Modelling (Geomodel), Saint Petersburg State University, Ulyanovskaya Str. 1, 198504 St. Petersburg, Russia

* Corresponding author



Me⁴⁺-bearing (Me⁴⁺ = Sn, Ti) dravite analogs were synthesized in the system MeO₂–MgO–Al₂O₃–B₂O₃–SiO₂–NaO–H₂O at 700 °C and 4/0.2 GPa in four hydrothermal experiments. Tourmalines form rosette-like aggregates and needle-like crystals that are chemically homogeneous. Tourmaline crystals obtained in high-pressure runs (4 GPa) are much smaller (up to 0.1 × 2 μm) and have lower Me⁴⁺ (0.27 wt. % SnO₂, 0.57 wt. % TiO₂) than those from the low-pressure (0.2 GPa) runs (up to 1 × 5 μm; 1.77 wt. % SnO₂, 2.25 wt. % TiO₂). Synthetic analogs of rutile, quartz and coesite were obtained in the system TiO₂–MgO–Al₂O₃–B₂O₃–SiO₂–NaO–H₂O, whereas synthetic analogs of cassiterite, tin-rich (up to ~19.55 wt. % SnO₂) Na-pyroxene, MgSn(BO₃)₂ (Mg-analogue of tusionite), quartz and coesite were synthesized in the system SnO₂–MgO–Al₂O₃–B₂O₃–SiO₂–NaO–H₂O. We suggest that at a high temperature (≥ 700 °C), the pressure negatively affects the Ti incorporation into the tourmaline structure. In contrast, at relatively low pressures, the Ti incorporation in tourmaline structures is governed by the Ti content in the mineral-forming medium. Low-pressure conditions are feasible for Sn incorporation in the tourmaline structure. The presence of Ti⁴⁺ and Sn⁴⁺ cations in structures of the synthesized tourmalines (probably at octahedrally coordinated sites), is also indicated by changes in the unit-cell parameters.

Keywords: tourmaline, pyroxene, jadeite, tin, titanium, hydrothermal synthesis

Received: 16 November 2021; **accepted:** 22 June 2022; **handling editor:** F. Bosi

1. Introduction

The tourmaline-supergroup minerals with generalized structural formula ${}^{[9]}X^{[6]}Y_3^{[6]}Z_6^{[4]}T_6O_{18} ({}^{[3]}BO_3)_3V_3W$ (Henry et al. 2011) are widespread in nature (Grew et al. 2017) and may form in various geological environments (e.g., Trumbull et al. 2008; Arif et al. 2010) under a wide range of thermodynamic conditions (London 2011; Setkova et al. 2019). Tourmaline is widely used not only as a geochemical recorder (e.g., van Hinsberg and Schumacher 2007; Marschall and Jiang 2011) but also as promising material with piezoelectric (e.g., Li et al. 2012) and pyroelectric properties (e.g., Chernyshova et al. 2021), and ultraviolet optical nonlinearity (Xia and Kang 2022).

The tourmaline crystal structure (space group *R3m*) may accommodate ca. ¼ from elements of the Periodic Table in significant amounts (> 1 wt. %; Vereshchagin et al. 2018). However, as natural tourmalines could contain up to 10 different cations at the same crystallographic site simultaneously (e.g., Ertl et al. 2019), data on synthetic tourmaline analogs are needed to determine (1) preferable crystallographic sites for each element, (2) maxi-

um contents of different cations, and (3) influence of *PT*-parameters on tourmaline composition, crystal structure and crystallization.

Recently, synthetic tourmalines were studied systematically, including those containing monovalent (Ag⁺, Li⁺, K⁺, NH₄⁺, Na⁺; London et al. 2006; Berryman et al. 2014, 2016; Wunder et al. 2015; Kutzschbach et al. 2017), divalent (Pb²⁺, Ca²⁺, Fe²⁺, Co²⁺, Ni²⁺, Cu²⁺; Rozhdestvenskaya et al. 2012; Vereshchagin et al. 2013, 2020), and trivalent cations (Cr³⁺, Fe³⁺; La³⁺, Nd³⁺, Eu³⁺, Yb³⁺, Ga³⁺; Vereshchagin et al. 2014, 2015, 2018, 2021). Studies on synthetic tourmalines that contain less frequent tetravalent cations are scarce (e.g., Ge⁴⁺-tourmaline; Pushcharovsky et al. 2020).

This work is focused on Ti⁴⁺- and Sn⁴⁺-bearing tourmalines. In relatively small amounts, tin and titanium are found in natural tourmalines: ~1.8 and 4.6 wt. % MeO₂, respectively (e.g., Vezzoni et al. 2018; Drivenes 2021). Nevertheless, they have high significance as titanium content in tourmaline correlates with bulk TiO₂ content of the host rock, and is a good indicator of magmatic evolution (e.g., da Costa et al. 2021). Furthermore, tin-bearing tourmalines are proposed as efficient indicators

Tab. 1 Synthesis conditions ($T = 700\text{ }^{\circ}\text{C}$, duration 8 days) and phase composition of synthesis products (PXRD data).

Synthesis conditions				Phase composition (PXRD)		
No	Run	Pressure, GPa	Dopant	Phase/Formula	ICSD	Content, %
1	3-1	4	TiO ₂	Tourmaline	98377	83
				Rutile	51930	11
				Coesite	54065	6
2	3-2	4	SnO ₂	Tourmaline	98377	80
				Jadeite	10232	7
				Cassiterite	154960	5
				MgSn(BO ₃) ₂	28266	4
3	3-3	0.2	TiO ₂	Coesite	54065	4
				Tourmaline	98377	79
				H ₃ BO ₃	52290	10
4	3-4	0.2	SnO ₂	Rutile	51930	8
				Quartz	41414	3
				Tourmaline	98377	83
				H ₃ BO ₃	52290	8
4	3-4	0.2	SnO ₂	Quartz	41414	3
				MgSn(BO ₃) ₂	28266	6
				Quartz	41414	3

of porphyry-style and granitoid-related Sn deposits (e.g., Mlynarczyk and Williams-Jones 2006; Baksheev et al. 2012, 2020).

The objectives of this work were: 1) to synthesize Ti⁴⁺ and Sn⁴⁺-bearing tourmalines; 2) to analyze the pressure effect on Me^{4+} ($Me^{4+} = Ti^{4+}, Sn^{4+}$) content of tourmalines, the morphology of crystals and the composition of associated phases; 3) to compare data on synthetic Me^{4+} -tourmalines and natural counterparts to correlate the experimental data with geological observations.

2. Materials and methods

2.1. Synthesis

Titanium- and Sn-bearing tourmaline analogs were synthesized in experiments with 8-day runtimes at the temperature of 700 °C and pressures of 0.2 and 4.0 GPa (Tab. 1). Hydrothermal pressure equipment (2 runs; at 0.2 GPa) and end-loaded piston-cylinder press (2 runs; at 4.0 GPa) were used. A homogeneous mixture of solid Na₂O, MgO, γ -Al₂O₃, SiO₂ (quartz) and H₃BO₃ in the atomic proportions of ideal dravite [NaMg₃Al₆(Si₆O₁₈)(BO₃)₃(OH)₃(OH)] was prepared, and then mixed with Ti or Sn (added as TiO₂ or SnO₂, respectively) in the oxide-to-dravite weight ratio of 1 : 10. Welded Au-capsules (10 mm length, 3 mm outer diameter, 0.25 mm wall thickness) for the piston-cylinder experiments (No 1 and 2, Tab. 1) were placed in pairs side by side in an assembly consisting of a steel furnace with NaCl as a pressure medium. The pressure was calibrated based on the quartz-coesite transition (Mirwald and Massonne 1980), which is accurate within 50 MPa. The temperature was measured

during all experiments with a Ni–CrNi thermocouple; its error is estimated to be $\pm 10\text{ }^{\circ}\text{C}$ (Schilling and Wunder 2004). At the end of the experiment, samples were quenched isobarically to a temperature below 200 °C in less than 15 seconds prior to the slow release of pressure. Welded Au-capsules (15–30 mm length, 3 mm outer diameter, 0.25 mm wall thickness) for the low-pressure experiments (No 3 and 4; Tab. 1) were placed in standard, cold-seal hydrothermal pressure vessels, with the pressure maintained within 10 MPa of the target pressure. After the experiment, the samples were

quenched by cooling the autoclave with compressed air to less than 100 °C in 5 min. Finally, the sample material was removed and prepared for analysis by powder X-ray diffraction, optical and scanning electron microscopy and electron microprobe analysis.

2.2. X-ray Diffraction

Powder X-ray diffraction (PXRD) patterns of newly-formed phases were recorded on an STOE StadiP diffractometer (CuK α ₁ radiation, curved Ge (111) monochromator, 40 kV accelerating voltage, 40 mA beam current, 2 θ range 5–125°, 0.01° scan step). Relative phase mass proportions (Tab. 1) were determined using the Rigaku PDXL v. 2.0 software. Unit-cell dimensions were determined by Rietveld refinement using the software package GSAS (Larson and VonDreele 1987). Initial structure parameters for dravite were taken from the Inorganic Structure Database (ICSD 98377, FIZ Karlsruhe). In the tourmaline structure-refinements ($T = \text{Si}; B = \text{B}; Z = \text{Al}, \text{Mg}; Y = \text{Al}, \text{Mg}, \text{Ti}, \text{Sn}; X = \text{Na}$), site-occupancy values as determined by electron microprobe analysis were used. Occupancies of Al and Mg at Y and Z sites were fixed.

2.3. Elemental Analysis

The composition and morphology of synthesized crystals were studied on the epoxy-mounted, polished, and carbon-coated samples utilizing a JEOL Hyperprobe JXA-8500F electron microprobe (EPMA) equipped with a thermal field-emission cathode and five wavelength-dispersive spectrometers (WDS) using 15 kV, 20 nA and a probe size appropriate to the size of the tourmaline

crystals. Large, radially arranged crystals were measured individually. Needles formed under HP conditions and <0.1 μm in size could only be measured completely in their rosette-shaped structure. Moreover, a Hitachi S-3400N scanning electron microscope (SEM) equipped with an AzTec Energy X-Max 20 energy dispersive spectrometer (EDS) was used for additional imaging. During EPMA quantitative analyses, the following analytical standards were used: Harvard schorl (Si, Al), jadeite (Na), diopside (Mg), cassiterite (Sn), and rutile (Ti). WDS raw data were processed by applying a $\phi(\rho Z)$ correction scheme (CITZAF; Armstrong 1995). To monitor possible peak shifts during measurements, the calibration material was analyzed before, during and after the analysis. Tourmaline structural formulae were calculated on the basis of 15 ($Y+Z+T$) atoms per formula unit (*apfu*), considering that: (1) vacancies may occur at the *X*-site, (2) no excess of boron ($B = 3 \text{ apfu}$), (3) tin and titanium occur at octahedrally coordinated sites. H₂O was calculated on the basis of an electroneutral formula as: ¹⁶O/OH ratio, based on $Y+Z+T=15 \text{ apfu}$. Pyroxene structure formulae were calculated based on 6 oxygen *apfu*.

3. Results

3.1. Phase composition and morphology of the run products

Synthetic tourmalines were the main phases in all four syntheses (78–83 vol. % of the resultant phase composition; Tab. 1) and occurred as rosette-like, acicular aggregates (Figs 1a, b) or elongated colorless crystals and their intergrowths (Figs 1c, d). Tourmaline crystals obtained in high-pressure experiments are much smaller (up to $0.1 \times 2 \text{ μm}$; Figs 1a, b) than those from the low-pressure runs (up to $1 \times 5 \text{ μm}$; Fig. 1c, d). Synthetic analogs of rutile, quartz and coesite were obtained in

Ti-experiments. Rutile was formed regardless of pressure conditions (runs 3-1 and 3-3; Tab. 1).

Synthetic analogs of cassiterite, pyroxene (jadeite – Sn-pyroxene solid solution), quartz, coesite along with MgSn(BO₃)₂ were produced along with tourmaline in Sn-experiments (runs 3-2 and 3-4; Tab. 1). The phase MgSn(BO₃)₂ occurred both in the high- and low-pressure experiments, but its proportion (Tab. 1) and morphology (Fig. 1) differ significantly. In the low-pressure experiment, MgSn(BO₃)₂ occurs as well-shaped elongated crystals (Fig. 1d), whereas it is rare and forms shapeless colloidal aggregates at high pressure. Cassiterite and pyroxene only occurred in the high-pressure experiment (No 3-2; Tab. 1).

3.2. Titanium and tin valence state in studied tourmalines

Both tin and titanium are present in the synthetic tourmalines as tetravalent cations; this is supported by the synthesis conditions and the composition of the run products. All synthesis runs were carried out under acid conditions (boric acid solution) with high oxygen fugacity using tetravalent precursors (TiO₂ and SnO₂); moreover, the oxidized conditions are indicated by all newly-formed by-product compounds (rutile, cassiterite, MgSn(BO₃)₂) that contain dominant Ti⁴⁺ or Sn⁴⁺.

Boric acid solution with high oxygen fugacity precludes divalent/trivalent titanium and divalent tin formation. Reports on divalent titanium are confined to solid-state compounds, and the aqueous chemistry of Ti²⁺ in F-free solutions is almost unknown. In acidic media, trivalent titanium is quite stable; however, unusually

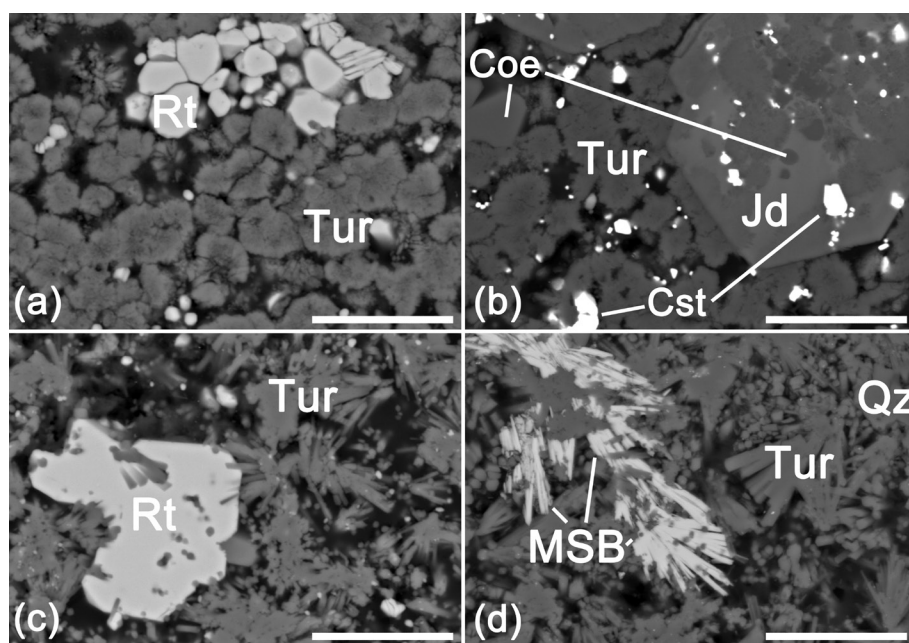


Fig. 1 BSE images of synthesis products, obtained at high (a, b) and low pressure: (c, d): a – tourmaline and rutile (run 3-1), b – tourmaline, Sn-rich pyroxene, coesite and cassiterite (run 3-2), c – tourmaline and rutile (run 3-3), d – tourmaline, quartz and MgSn(BO₃)₂ (run 3-4). Abbreviations: Tur – tourmaline, Rt – rutile, Coe – coesite, Cst – cassiterite, Jd – Sn-rich pyroxene, Qz – quartz, MSB – MgSn(BO₃)₂. The scale bar is 20 μm. Mineral symbols, according to Warr (2021).

Tab. 2 Chemical composition (wt. %) and atomic ratios (*apfu*) of synthetic tourmalines and pyroxenes and unit-cell parameters (Å) of synthetic tourmalines.

Component	tourmaline				pyroxene			
	3-1	3-3	3-2	3-4	3-2*			
SiO ₂	37.45	36.93	36.11	37.43	57.25	53.55		
Al ₂ O ₃	34.55	33.43	35.92	34.01	23.86	9.41		
MgO	10.63	11.08	10.46	11.03	2.11	5.45		
TiO ₂	0.57	2.27	–	–	–	–		
SnO ₂	–	–	0.27	1.77	3.20	19.55		
Na ₂ O	2.41	2.78	2.91	2.71	13.29	13.16		
H ₂ O _{calc}	3.54	3.43	3.59	3.53	–	–		
B ₂ O _{3scale}	10.94	10.95	10.91	10.97	–	–		
Total	100.10	101.01	100.16	101.44	100.01	101.12		
Calculated	15 (<i>T + Y + Z</i>) <i>apfu</i>				6 oxygen <i>apfu</i>			
<i>X</i>	Na	0.74	0.86	0.90	0.83	Na	0.88	0.96
	□	0.26	0.14	0.10	0.17	<i>M1</i> Mg	0.11	0.04
	Sum	1.00	1.00	1.00	1.00	Sum	0.99	1.00
<i>Y+Z</i>	Al	6.41	6.11	6.50	6.28	Al	0.92	0.41
	Mg	2.52	2.62	2.48	2.61	Mg	0.00	0.26
	Ti	0.07	0.27	–	–	<i>M2</i> Ti	–	–
	Sn	–	–	0.02	0.11	Sn	0.04	0.29
Sum	9.00	9.00	9.00	9.00	Sum	0.96	0.96	
<i>T</i>	Si	5.95	5.86	5.75	5.93	Si	1.96	2.01
	Al	0.05	0.14	0.25	0.07	<i>T</i> Al	0.04	–
	Sum	6.00	6.00	6.00	6.00	Sum	2.00	2.01
<i>V+W</i>	O	0.24	0.36	0.18	0.27			
	OH	3.76	3.64	3.82	3.73			
Sum	4.00	4.00	4.00	4.00				
<i>a</i>	15.903(1)	15.921(1)	15.908(3)	15.903(1)				
<i>c</i>	7.169(1)	7.177(1)	7.175(2)	7.168(1)				
<i>V</i>	1570.3(3)	1575.5(3)	1574.6(6)	1570.0(3)				

* – data from pyroxene zones with minimum and maximum content provided.

strong reducing conditions must be present to produce Ti³⁺ (e.g., Ma and Rossman 2009). Up to date, only four Ti³⁺-dominant minerals are known (tistarite, kaitianite, grossmanite and colomeraite), which were all found in meteorites or in ultra-low oxygen fugacity assemblages. In aqueous solutions, both divalent and tetravalent tin could exist as complex ions. However, pronounced reducing conditions are necessary to produce Sn²⁺ from Sn⁴⁺. Up to date, only six Sn²⁺-dominated minerals are known (abhurite, foordite, hydromarchite, romarchite, stanmicrolite, and thoreaulite). Conditions of exceptionally low oxygen fugacity are required for their formation (e.g., Černý et al. 1988). Alternatively, Sn²⁺ could be derived from corrosion of tin or bronze (e.g., Ramik et al. 2003), which is also not our case.

3.3. Chemical composition of the run products

No chemical zonation was observed in the obtained tourmalines. Based on the EPMA data that indicate ³Na ~ 1 atoms per formula unit (*apfu*), ^{Y+Z}Al > 6 *apfu*, ^{Y+Z}Mg > 2 *apfu*, and ^WOH > ^WO (Tab. 2), all obtained tourma-

lines are synthetic analogs of dravite species. Depending on the pressure conditions, the obtained tourmalines contain from 0.57 to 2.25 wt. % TiO₂ (runs 3-1, 3-3, respectively) or from 0.27 to 1.77 wt. % SnO₂ (runs 3-2, 3-4, respectively). In all cases, tourmalines obtained at low-pressure conditions contain more Me⁴⁺ than those obtained by high-pressure synthesis.

As tourmalines were the main products in all synthesis runs (Tab. 1), it was possible to collect powder X-ray data in sufficient quality to calculate the tourmaline unit-cell parameters (u.c.p.). The synthesized tourmalines (Tab. 2) have lower *a* and similar *c* parameters compared to natural dravite (*a* ~ 15.946, *c* ~ 7.172 Å; Pertlik et al. 2003); with an increase in the contents of Me⁴⁺ cations, their *a* and *c* parameters either increase or decrease. In Ti-tourmalines, where the Ti contents increase from 0.07 to 0.27 *apfu*, both *a* and *c* increase (*a* by 0.018 Å and *c* by 0.008 Å); on the other

hand, in Sn-tourmalines, where Sn contents increase from 0.02 to 0.11 *apfu*, both *a* and *c* parameters decrease (*a* by 0.005, *c* by 0.007 Å). The changes of all parameters exceed their respective errors, i.e., the observed changes are significant.

The synthetic Na-pyroxene analog has various SnO₂ contents (from 3.20 to 19.55 wt. % SnO₂; Tab. 2) in different crystal zones; in most cases, Sn-enrichment was found in inner zones of pyroxene crystals (Fig. 1). No chemical zonation that could be traced by EMPA was observed in all other phases (quartz, coesite, MgSn(BO₃)₂, rutile and cassiterite).

4. Discussion

4.1. Titanium-enriched tourmalines

Titanium-bearing tourmalines from high- and low-pressure experiments differ significantly in titanium content and morphology. As the Ti content in synthetic tourmalines from the low-pressure experiment (run 3-3; Tab. 2) is higher compared to the high-pressure one (run

3-1; Tab. 2), we found out that a pressure increase influences the titanium content negatively in our synthetic tourmalines. The well-shaped tourmaline crystals (up to 500 µm) from the Kreuzeck Mountains contain rutile (TiO₂) and fluorapatite (Ca₅(PO₄)₃F) inclusions (Konzett et al. 2012). This observation could indicate (1) an elevated Ti and F content in the system and/or (2) Ti-enrichment of tourmaline by recrystallization at the late rock-forming stage. Fluorine content is known to enhance rutile crystallization along the specific facets (e.g., Lai et al. 2013) and thus can affect Ti-content in tourmaline by fractionation effects. In the products of both syntheses, titanium oxide (rutile) is present, but it is rarer in the low-pressure experiment. It is worth noting that in the low-pressure experiment (run 3-3; Tab. 1) well-shaped elongated tourmaline crystals spike intergrowths of rutile crystals, which indicate tourmaline crystallization prior to rutile (Fig. 1c). Further, Ti content in tourmaline is almost 4-times higher in the LP than in the HP experiment. In the case of the high-pressure experiment (run 3-1; Tab. 1), acicular tourmaline and octahedron-like rutile are two separate phases with no clear evidence of crystallization sequence (Fig. 1a). This suggests that pressure affects the incorporation of titanium into the synthesized tourmalines indirectly, by controlling the rutile content and the availability of Ti from the system.

Our data show, that synthetic tourmalines could contain up to 2.27 wt. % TiO₂, which is quite a high value, but which is still smaller than found in some natural tourmalines. Among the Ti-richest tourmalines are those with 4.62 wt. % TiO₂ in massive porphyritic rocks of the Alpi Apuane in Italy (Vezzoni et al. 2018), 3.80 wt. % TiO₂ in pegmatites of the Třebíč Pluton in Czech Republic (Novák et al. 2011); 3.60 wt. % TiO₂ in meta-evaporite in Alto Chapare, Cochabamba in Bolivia (Žáček et al. 2000); and 3.42 wt. % TiO₂ in eclogites from the Kreuzeck Mountains, Eastern Alps in Austria (Konzett et al. 2012). Review on titanium in tourmalines from granitic pegmatites and their exocontacts provided in Gadas et al. (2019), while Ti-bearing, Al-deficient tourmaline assemblage associated with lamprophyre dikes (O'Grady Batholith, Canada) described in Scribner et al. (2018), where authors emphasize the Al-deficiency as the key common feature of all Ti-rich tourmalines. It is worth noting that Ti-rich tourmaline species, dutrowite, was recently approved (IMA 2019-082; Biagioni et al. 2020). Tourmalines from the high-pressure high temperature (HPHT) experiment (run 3-1; Tab. 2) contain much smaller amounts of titanium than tourmalines found in eclogites, which were formed at 2 GPa and 650 °C (Konzett et al. 2012). Data from Žáček et al. (1998) suggest that tourmalines, including Ti-rich varieties, associated with rutile at Alto Chapare were formed at relatively low temperature and pressure. Taking into account the

geochemical signature (Be, REE, Ti, U, Th, Zr, Nb > Ta, F) (Zachář et al. 2020), the NYF pegmatites of the Třebíč Pluton, Czech Republic, hold Ti-rich dravite possibly replacing titanite and ilmenite (Novák et al. 2011), which were formed at relatively low temperature and pressure (500–650 °C and 0.1–0.2 GPa; Zachář et al. 2020). The Ti concentration in tourmalines from altered rocks of hydrothermal deposits formed at lower temperature and pressure is highly variable. This depends probably on the chemical composition of the replaced rock. For example, at the Berezovskoe gold deposit in the Central Urals, Russia, formed over the temperature and pressure ranges ~250–370 °C and 0.1–0.3 GPa, respectively (Baksheev et al. 2001; Vikent'eva et al. 2017), the Ti content in dravite from altered gabbro and ultramafic rock ranges from 0.11 to 1.24 and from the detection limit to 0.31 wt. % TiO₂, respectively (Kudryavtseva and Baksheev 2003).

Summarizing our experimental data and literature data on natural Ti-rich tourmalines, we tentatively suggest that at high T ($\geq 700^\circ\text{C}$), the pressure negatively affects the Ti incorporation into the tourmaline structure. In contrast, at relatively low pressures, the Ti incorporation in tourmaline structures is governed by the Ti content in the mineral-forming medium.

There is no direct information on titanium speciation in the tourmaline crystal structure. However, both natural observations (e.g., Žáček et al. 2000; Konzett et al. 2012) and our data on synthetic tourmalines (EMPA and u.c.p.) indicate that titanium most likely occupies octahedrally coordinated sites in the tourmaline crystal structure according to the substitution: $2^{Y,Z}\text{Al}^{3+} \leftrightarrow ^{Y,Z}\text{Ti}^{4+} + ^{Y,Z}\text{Mg}^{2+}$. Data on Ti-rich tourmalines from meta-evaporite in Alto Chapare, Cochabamba, Bolivia (Žáček et al. 2000) are indicating that Ti⁴⁺ incorporation in tourmaline is coupled with a decrease of OH and an increase of O. This pattern, which is also typical for our synthetic Ti-tourmalines (Tab. 2), indicates the following substitution scheme: $^{Y,Z}\text{Al}^{3+} + ^{Y,W}\text{OH}^- \leftrightarrow ^{Y,Z}\text{Ti}^{4+} + ^{Y,W}\text{O}^{2-}$. Both schemes should lead to an increase in unit-cell parameters with an increasing titanium content ($r_{\text{Mg}} > r_{\text{Ti}} > r_{\text{Al}}$; Shannon 1976), which was actually observed in our samples (Tab. 2). Thus, changes of the u.c.p. values confirm the incorporation of titanium ions into the synthesized tourmalines.

4.2. Tin-enriched tourmalines

Our study of synthesized Sn-bearing tourmalines showed that their Sn content also increases with decreasing pressure and can reach 1.77 wt. % SnO₂. It is known that tin content in tourmalines, which were found in several hydrothermal deposits, varies significantly. In tourmalines from Nanjizal, Land's End in England, it is 2.48 wt. % SnO₂ (Drivenes 2021); in Solnechnoe in Russia – 1.02 wt. % SnO₂; (Baksheev et al. 2020); in Pridorozhnoe in

Russia – 0.96 wt. % SnO₂ (Baksheev et al. 2012); in Kidd Creek in Canada – 0.46 wt. % SnO₂ (Slack et al. 1999); in San Rafael in Peru – 0.38 wt. % SnO₂ (Mlynarczyk and Williams-Jones 2006); and in Roche in England – 0.35 wt. % SnO₂ (Williamson et al. 2000). Therefore, the maximum content of tin in natural tourmalines from hydrothermal deposits and synthetic samples obtained at 700 °C at a pressure of 0.2 GPa is similar (~2 wt. % SnO₂), although natural hydrothermal tourmalines precipitated at much lower temperatures.

In our HPHT experiment, the tin content in tourmalines reaches only 0.27 wt. % SnO₂ (Tab. 2). Cassiterite (along with coesite) was found inside (1) well-shaped poikilitic pyroxene crystals and (2) MgSn(BO₃)₂ aggregates and (3) between acicular tourmaline crystals (Fig. 1b), which indicates its precipitation at the first stage of crystallization. Pyroxene crystals are surrounded by rosette-like tourmalines, which shows their crystallization prior to tourmaline. Tourmalines form acicular aggregates that are overgrowing tin-rich pyroxene (up to ~19.55 wt. % SnO₂), possibly precipitated after cassiterite. This could explain the low Sn content (0.02 *apfu*) in the tourmalines. In addition, Sn incorporated into MgSn(BO₃)₂ (Tab. 1) could also decrease the availability of Sn for tourmaline. No direct analogs of obtained synthetic assemblage have been found in nature yet, but synthesis products resemble the composition of tin slags (e.g., Butler 1978). Previously, tin-rich pyroxene (aluminous hedenbergite with ~12 wt. % SnO₂) was reported from a high-temperature (>1100 °C) Sn-bearing slag in association with tin-rich garnet, spinel and cassiterite (Butler 1978). Our data show that Na-pyroxene can host sufficient amounts of tin (up to 0.29 *apfu*), and Sn-rich pyroxene could occur in HPHT rocks.

Tourmaline from low-pressure, high-temperature experiments has a much higher Sn content (1.77 wt. % SnO₂) compared to HPHT tourmaline (Tab. 2). It is associated with quartz and MgSn(BO₃)₂ (Tab. 1). It is noteworthy to mention that previously MgSn(BO₃)₂ was synthesized at 1000 °C (Aléonard and Vicat 1966) / 500 °C (Nekrasov et al. 1970). This phase is an Mg-analogue of tusionite mineral (Konovalenko et al. 1984; Cooper et al. 1994). Tusionite was found in granitic pegmatites in association with elbaite, danburite, hambergite and quartz, containing up to ~1 wt. % MgO, and is replaced by cassiterite (Cooper et al. 1994). In our low-pressure experiment, cassiterite is not precipitated and tin is concentrated in tourmaline and “tusionite-Mg”. We believe that high temperature at relatively low pressure (0.2 GPa) negatively affects cassiterite precipitation, although the pressure is close to that of rare-metal pegmatites, where cassiterite is a typical mineral.

Data on tin slags (Butler 1978) along with our data on HPHT hydrothermal synthesis (Tab. 1) indicate that

tin preferably partitions into pyroxene (up to ~20 wt. % SnO₂) at HP conditions, whereas under low-pressure, high-temperature conditions (LPHT) it partitions into tourmalines (up to ~2 wt. % SnO₂). Published data on natural Sn-rich tourmaline (see above) testify to its formation in relatively low-temperature low-pressure (LPLT) environments. For example, at the San Rafael deposit, the Sn-bearing tourmaline associated with cassiterite could precipitate over the temperature range of ~270–360 °C (Mlynarczyk and Williams-Jones 2006) and pressure of 0.2 GPa (Kontak and Clark 2002). Ore-stage minerals, including Sn-rich schorl, were precipitated at the Solnechoe hydrothermal Sn-deposit at 300–400 °C (Bannikova et al. 1994). These published data are testimony that LPLT conditions are feasible for Sn incorporation into the tourmaline structure. Thus, tin ions incorporate into the tourmaline structure under low-pressure conditions, independent of the temperature.

Our data on tin-tourmaline and tin-pyroxene (Tab. 2), data on tin-tourmaline (Baksheev et al. 2020), and coexisting tin-free melilite and tin-enriched pyroxene (Butler 1978), suggest that Sn⁴⁺ occupies octahedral sites in the tourmaline and pyroxene crystal structures. Baksheev et al. (2020) pointed out that, despite the Si content variation in Sn-bearing schorl, no correlation between Si and Sn was found and suggested the substitution scheme for the Sn-bearing schorl as follows: ${}^X\text{Ca}^{2+} + {}^{YZ}\text{Fe}^{2+} + {}^{YZ}\text{Al}^{3+} \leftrightarrow {}^X\text{Na}^{+} + {}^{YZ}\text{Mg}^{2+} + {}^{YZ}\text{Sn}^{4+}$ (Baksheev et al. 2020).

Based on chemical data and the ratios of the ionic radii of octahedral cations coexisting in the same crystal ($r_{\text{Mg}} > r_{\text{Sn}} > r_{\text{Al}}$; Shannon 1976), the observed insignificant decrease of the u.c.p. values with increasing tin content (Tab. 2) can be explained by assuming that the entry of Sn-ions into tourmalines occurs not only according to previously discussed schemes (see text above; $2{}^{YZ}\text{Al}^{3+} \leftrightarrow {}^{YZ}\text{Sn}^{4+} + {}^{YZ}\text{Mg}^{2+}$; ${}^{YZ}\text{Al}^{3+} + {}^{VW}\text{OH}^{-} \leftrightarrow {}^{YZ}\text{Sn}^{4+} + {}^{VW}\text{O}^{2-}$), but also according to an additional scheme: $2{}^{YZ}\text{Mg}^{2+} = {}^{YZ}\text{Sn}^{4+} + {}^{YZ}\text{vacancy}$. Unlike the first two schemes, the latter leads to a decrease in u.c.p. due to a decrease in Mg content and an increase in Sn content.

Summarizing our experimental data and published data on natural Sn-rich tourmalines, we conclude that the Sn concentration in tourmaline depends in general on the Sn content of the tourmaline-forming medium. The PT parameters control the composition of the phases which co-exist with tourmaline, including phases in which Sn is present, either as a major or minor element.

5. Conclusions

Me^{4+} ($Me^{4+} = \text{Sn, Ti}$) bearing dravites were synthesized in the system $MeO_2\text{--MgO--Al}_2\text{O}_3\text{--B}_2\text{O}_3\text{--SiO}_2\text{--NaO--H}_2\text{O}$ under hydrothermal conditions of 700 °C and 4/0.2 GPa.

The incorporation of Ti⁴⁺ and Sn⁴⁺ ions into the synthesized tourmalines is confirmed by changes of the unit cell parameters. It was found that a pressure increase reduces the maximum content of Me⁴⁺ in tourmalines and the size of the synthesized crystals and also affects the resulting assemblage of different phases. The incorporation of Ti and Sn ions into the synthesized tourmalines is confirmed by changes in the unit-cell parameters.

Divalent (Pb, Ca, Fe, Co, Ni, Cu) and trivalent cations (Cr, Fe; La, Nd, Eu, Yb, Ga) can easily incorporate into the tourmaline crystal structure in a rather low-pressure regime. In this study, we show that this is also the case for tetravalent cations (Sn, Ti). It is clear that enhanced incorporation of a trace element points to enrichment of that element in the system. Our experiments combined with literature data indicate that enhanced tourmaline growth occurs at a low pressure, independent of the temperature. This is of general interest to use abundant tourmaline as an indicator mineral in shallow or uppermost crust environments.

Acknowledgments. The authors thank U. Dittmann for sample preparation, H.-P. Nabein for help with the PXRD analysis and resource centers of SPbSU (Centre for X-ray Diffraction Studies and Geomodel) for providing instrumental and computational resources. We are thankful to the Guest Editors, Ferdinando Bosi and Jan Cempírek, and two reviewers, anonymous and Andreas Ertl, who contributed significantly to improving the quality of the manuscript. This work was supported by the grant of the President of the Russian Federation MK-1832.2021.1.5.

References

- ALÉONARD S, VICAT J (1966) Borates de structure dolomite. *Bull Soc franç Minéral Cristallogr* 89: 271–272
- ARIF M, HENRY DJ, MOON CJ (2010) Cr-bearing tourmaline associated with emerald deposits from Swat, NW Pakistan: Genesis and its exploration significance. *Amer Miner* 95: 799–809
- ARMSTRONG JT (1995) CITZAF: a package of correction programs for the quantitative electron microbeam X-ray-analysis of thick polished materials, thin films, and particles. *Microbeam Anal* 4: 177–200
- BAKSHEEV IA, PROKOF'EV VY, USTINOV VI (2001) Genesis of metasomatic rocks and mineralized veins at the Berzovskoe deposit, Central Urals: Evidence from fluid inclusions and stable isotopes. *Geochem Int* 39: S129–S144
- BAKSHEEV IA, PROKOF'EV VY, ZARAIISKY GP, CHITALIN AF, YAPASKURT VO, NIKOLAEV YN, TIKHOMIROV PL, NAGORNAYA EV, ROGACHEVA LI, GORELIKOVA NV, KONONOV OV (2012) Tourmaline as a prospecting guide for the porphyry-style deposits. *Eur J Mineral* 24:957–979
- BAKSHEEV IA, VIGASINA MF, YAPASKURT VO, BRYZGALOV IA, GORELIKOVA NV (2020) Tourmaline from the Solnechnoe tin deposit, Khabarovsk Krai, Russia. *Mineral Mag* 84:245–265
- BANNIKOVA LA, SUSHCHEVSIKAYA T, SPAENNYKH MY, BARSUKOV VL (1994) Isotopic and geochemical study of the conditions of tin ore formation of Solnechnoye deposit (Far East of Russia). *Geochem J* 28: 411–428
- BERRYMAN EJ, WUNDER B, ERTL A, KOCH-MÜLLER M, RHEDE D, SCHEIDL K, GIESTER G, HEINRICH W (2016) Influence of the X-site composition on tourmaline's crystal structure: investigation of synthetic K-dravite, dravite, oxy-uvite, and magnesio-foitite using SREF and Raman spectroscopy. *Phys Chem Miner* 43: 83–102
- BERRYMAN EJ, WUNDER B, RHEDE D (2014) Synthesis of K-dominant tourmaline. *Amer Miner* 99:539–542
- BIAGIONI C, BOSI F, MAURO D, SKOGBY H, DINI A, ZACCARINI F (2020) Dutrowite, IMA 2019-082. *CNMNC Newsletter* 53, *Eur J Mineral* 32 <https://doi.org/10.5194/ejm-32-209-2020>.
- BUTLER BCM (1978) Tin-rich garnet, pyroxene, and spinel from a slag. *Mineral Mag* 42:487–492
- ČERNÝ P, FRANSOLET A-M, ERCIT TS, CHAPMAN R (1988) Foordite SnNb₂O₆, a new mineral species, and the foordite–thoreaulite series. *Canad Mineral* 26: 889–898
- CHERNYSHOVA IA, VERESHCHAGIN OS, MALYSHKINA OV, GONCHAROV AG, KASATKIN IA, MURASHKO MN, ZOLOTAREV AA, FRANK-KAMENETSKAYA OV (2021) Tourmalines pyroelectric effect depending on the chemical composition and cation oxidation state. *J Solid State Chem* 303: 122512 <https://doi.org/10.1016/j.jssc.2021.122512>
- COOPER M, HAWTHORNE F, NOVÁK M, TAYLOR MC (1994) The crystal structure of tusionite, Mn²⁺Sn⁴⁺(BO₃)₂, a dolomite-structure borate. *Canad Mineral* 32: 903–907
- DA COSTA IR, ANTUNES IMHR, RÉCIO C (2021) The Mg/(Fe+Mg) ratio and the Ti and A site contents of tourmaline as promising indicators of granitic magma evolution. *J Iber Geol* 47:307–321
- DRIVENES K (2021) Sn-rich tourmaline from the Land's End granite, SW England. In: *TUR2021 3rd International Conference on Tourmaline*. pp 27–28
- ERTL A, TOPA D, GIESTER G, ROSSMAN GR, TILLMANN E, KONZETT J (2019) Sr-bearing high-pressure tourmaline from the Kreuzeck Mountains, Eastern Alps, Austria. *Eur J Mineral* 31:791–798
- GADAS P, NOVÁK M, ŠKODA R, CEMPÍREK J, ZACHAŘ A, FLÉGR T, PEZZOTTA F (2019) Titanium in tourmalines from granitic pegmatites and their exocontacts. *Canad Mineral* 57 (5): 745–747
- GREW ES, HYSTAD G, HAZEN RM, KRIVOVICHEV SV, GORELOVA LA (2017) How many boron minerals occur in Earth's upper crust? *Amer Miner* 102: 1573–1587
- HENRY DJ, NOVÁK M, HAWTHORNE FC, ERTL A, DUTROW BL, UHER P, PEZZOTTA F (2011) Nomenclature of

- the tourmaline-supergroup minerals. *Amer Miner* 96: 895–913
- KONOVALENKO SI, VOLOSHIN AV, PAKHOMOVSKIY YA, ANEN'YEV SS, PERLINA GA, ROGACHEV DL, KUZNETSOV VY (1984) Tusionite $MnSn(BO_3)_2$ – a new borate from granitic pegmatites of the southwest Pamirs. *Int Geol Rev* 26: 481–485
- KONTAK DJ, CLARK AH (2002) Genesis of the Giant, Bonanza San Rafael Lode Tin Deposit, Peru: Origin and Significance of Pervasive Alteration. *Econ Geol* 97: 1741–1777
- KONZETT J, KRENN K, HAUZENBERGER C, WHITEHOUSE M, HOINKES G (2012) High-pressure tourmaline formation and fluid activity in Fe–Ti-rich eclogites from the Kreuzeck Mountains, Eastern Alps, Austria. *J Petrol* 53: 99–125
- KUDRYAVTSEVA OE, BAKSHEEV IA (2003) Compositional variations in tourmalines of the Berezovskoe gold deposit, Central Urals. *Zap Ross Miner O-va* 3: 108–125 (in Russian)
- KUTZSCHBACH M, WUNDER B, KRSTULOVIC M, ERTL A, TRUMBULL R, ROCHOLL A, GIESTER G (2017) First high-pressure synthesis of rossmanitic tourmaline and evidence for the incorporation of Li at the X site. *Phys Chem Miner* 44: 353–363
- LARSON A.C., VON DREELE R.B. (1987) Generalized structure analysis system. LosAlamos National Laboratory Report LAUR: 86-748.
- LAI Z, PENG F, WANG H, YU H, ZHANG S, ZHAO H (2013) A new insight into regulating high energy facets of rutile TiO_2 . *J Mater Chem A* 1: 4182–4185
- LI Y, HUANG Z, LIU Y, FANG M (2012) Characterization of dielectric performance of tourmaline single crystals from Yunnan, China. *CrystEngComm* 14: 7153–7156
- LONDON D (2011) Experimental synthesis and stability of tourmaline: a historical overview. *Canad Miner* 49: 117–136
- LONDON D, ERTL A, HUGHES JM, MORGAN VI GB, FRITZ EA, HARMS BS (2006) Synthetic Ag-rich tourmaline: structure and chemistry. *Amer Miner* 91: 680–684
- MA C, ROSSMAN GR (2009) Tistarite, Ti_2O_3 , a new refractory mineral from the Allende meteorite. *Amer Miner* 94: 841–844 <https://doi.org/10.2138/am.2009.3203>
- MARSCHALL H, JIANG S-Y (2011) Tourmaline isotopes: no element left behind. *Elements* 7: 313–319
- MIRWALD PW, MASSONNE H-J (1980) Quartz-coesite transition and the comparative friction measurements in piston-cylinder apparatus using talc-alsimag-glass (TAG) and NaCl high pressure cell: A discussion. *Neu Jb Mineral, Mh* 10: 469–477
- MLYNARCZYK M, WILLIAMS-JONES AE (2006) Zoned tourmaline associated with cassiterite: Implications for fluid evolution and tin mineralization in the San Rafael Sn-Cu deposit, southeastern Peru. *Canad Mineral* 44: 347–365
- NEKRASOV IY, GRIGORIEV AP, GRIGORIEVA TA, BROVKIN AA, DIMAN EN, NOVGORODOV IG, SUKNEV VS, NIKISHOVA LV (1970) Study of high-temperature borates. Nauka. Moscow, pp 1–288
- NOVÁK M, ŠKODA R, FILIP J, MACEK I, VACULOVÍČ T (2011) Compositional trends in tourmaline from intragranitic NYF pegmatites of the Třebíč pluton, Czech Republic: an electron microprobe, Mössbauer and LA-ICP-MS study. *Canad Mineral* 49: 359–380
- PERTLIK F, ERTL A, KÖRNER W, BRANDSTÄTTER F, SCHUSTER R (2003) Na-rich dravite in the marbles from Friesach, Carinthia, Austria: Chemistry and crystal structure. *Neu J Mineral, Mh* 6:277–288
- PUSHCHAROVSKY DY, ZUBKOVA NV, SETKOVA TV, BALITSKII VS, NEKRASOV AN, NESTEROVA VA (2020) (Ga,Ge)-analogue of tourmaline: crystal structure and composition. *Crystallogr Rep* 65: 849–856
- RAMIK RA, ORGAN RM, MANDARINO JA (2003) On type romarchite and hydromarchite from Boundary Falls, Ontario, and notes on other occurrences. *Canad Mineral* 41: 649–657
- ROZHDESTVENSKAYA IV, SETKOVA TV, VERESHCHAGIN OS, SHTUKENBERG AG, SHAPOVALOV YB (2012) Refinement of the crystal structures of synthetic nickel- and cobalt-bearing tourmalines. *Crystallogr Rep* 57: 57–63
- SETKOVA TV, BALITSKY VS, SHAPOVALOV YB (2019) Experimental study of the stability and synthesis of the tourmaline supergroup minerals. *Geochem Int* 57: 1082–1094
- SHANNON RD (1976) Revised effective ionic radii and systematic studies of interatomic distances in halides and chalcogenides. *Acta Crystallogr A* 32: 751–767
- SCHILLING F, WUNDER B (2004) Temperature distribution in piston-cylinder assemblies: Numerical simulations and laboratory experiments. *Eur J Mineral* 16: 7–14
- SCRIBNER ED, GROAT LA, CEMPÍREK J (2018) Mineralogy of Ti-bearing, Al-deficient tourmaline assemblages associated with lamprophyre dikes near the O'Grady Batholith, Northwest Territories, Canada. *J Geosci* 63 (2): 123–135
- SLACK JF, RAMSDEN AR, GRIFFIN WL, WIN TT, FRENCH DH, RYAN CG (1999) Trace elements in tourmaline from the Kidd Creek Massive Sulfide Deposit and Vicinity, Timmins, Ontario: a proton microprobe study. In: HANNINGTON MD, BARRIE CT (eds) *The Giant Kidd Creek Volcanogenic Massive Sulfide Deposit, Western Abitibi Subprovince, Canada*. Society of Economic Geologists, pp 415–430
- TRUMBULL RB, KRIENITZ M-S, GOTTESMANN B, WIEDENBECK M (2008) Chemical and boron-isotope variations in tourmalines from an S-type granite and its source rocks: the Erongo granite and tourmalinites in the Damara Belt, Namibia. *Contrib Mineral Petrol* 155: 1–18
- VAN HINSBERG V, SCHUMACHER J (2007) Intersector element partitioning in tourmaline: A potentially powerful single crystal thermometer. *Contrib Mineral Petrol* 153: 289–301

- VEZZONI, S, BIAGIONI C, D'ORAZIO M, PIERUCCIONI D, GALANTI Y, PETRELLI M., MOLLI G (2018) Evidence of Permian magmatism in the Alpi Apuane metamorphic complex (Northern Apennines, Italy): New hints for the geological evolution of the basement of the Adria plate. *Lithos*, 318–319, 104–123
- VERESHCHAGIN OS, ROZHDESTVENSKAYA IV, FRANK-KAMENETSKAYA OV, ZOLOTAREV AA, MASHKOVITSEV RI (2013) Crystal chemistry of Cu-bearing tourmalines. *Amer Miner* 98: 1610–1616
- VERESHCHAGIN OS, ROZHDESTVENSKAYA IV, FRANK-KAMENETSKAYA OV, ZOLOTAREV AA (2014) Ion substitutions and structural adjustment in Cr-bearing tourmalines. *Eur J Mineral* 26:309–321
- VERESHCHAGIN OS, FRANK-KAMENETSKAYA OV, ROZHDESTVENSKAYA IV (2015) Crystal structure and stability of Ni-rich synthetic tourmaline. Distribution of divalent transition-metal cations over octahedral positions. *Mineral Mag* 79: 997–1006
- VERESHCHAGIN OS, FRANK-KAMENETSKAYA OV, ROZHDESTVENSKAYA IV, ZOLOTAREV AA (2018) Incorporation of 3d elements in tourmalines: structural adjustments and stability. *Eur J Mineral* 30: 917–928
- VERESHCHAGIN OS, WUNDER B, BRITVIN SN, FRANK-KAMENETSKAYA OV, WILKE FDH, VLASENKO NS, SHILOVSKIKH VV (2020) Synthesis and crystal structure of Pb-dominant tourmaline. *Amer Miner* 105: 1589–1592
- VERESHCHAGIN OS, BRITVIN SN, WUNDER B, FRANK-KAMENETSKAYA OV, WILKE FDH, VLASENKO NS, SHILOVSKIKH VV, BOCHAROV VN, DANILOV DV (2021) Ln³⁺ (Ln³⁺ = La, Nd, Eu, Yb) incorporation in synthetic tourmaline analogues: Towards tourmaline *REE* pattern explanation. *Chem Geol* 584: 120526 <https://doi.org/10.1016/j.chemgeo.2021.120526>
- VIKENTYEVA OV, BORTNIKOV NS, VIKENTYEV IV, GROZNOVA EO, LYUBIMTSEVA NG, MURZIN VV (2017) The Berezovsk giant intrusion-related gold-quartz deposit, Urals, Russia: Evidence for multiple magmatic and metamorphic fluid reservoirs. *Ore Geol Rev* 91: 837–863
- WARR LN (2021) IMA–CNMNC approved mineral symbols. *Mineral Mag* 85: 291–320
- WILLIAMSON BJ, SPRATT J, ADAMS JT, TINDLE AG, STANLEY CJ (2000) Geochemical constraints from zoned hydrothermal tourmalines on fluid evolution and Sn mineralization: an example from fault breccias at Roche, SW England. *J Petrol* 41: 1439–1453
- WUNDER B, BERRYMAN E, PLESSEN B, RHEDE D, KOCHMÜLLER M, HEINRICH W (2015) Synthetic and natural ammonium-bearing tourmaline. *Amer Miner* 100: 250–256
- XIA M, KANG L (2022) Tourmaline with ultraviolet optical nonlinearity: Emergent material discovery from mineral. *J Alloys Compd* 892: 162235
- ŽÁČEK V, PETROV A, HYRŠL J (1998) Chemistry and origin of povondraite-bearing rocks from Alto Chapare, Cochabamba, Bolivia. *J Czech Geol Soc* 43: 59–67
- ŽÁČEK V, FRÝDA J, PETROV A, HYRŠL J (2000) Tourmalines of the povondraite - (oxy)dravite series from the cap rock of meta-evaporite in Alto Chapare, Cochabamba, Bolivia. *J Czech Geol Soc* 45: 3–12
- ZACHAŘ A, NOVÁK M, ŠKODA R (2020) Beryllium minerals as monitors of geochemical evolution from magmatic to hydrothermal stage; examples from NYF pegmatites of the Třebíč Pluton, Czech Republic. *J Geosci* 65: 153–172

